Thermal Analysis: VCSELs on an SiOB

C. C. Chen, Y. C. Chen, Chin-Ta Chen, Hsu-Liang Hsiao, Chia-Chi Chang, Y. T. Cheng, *Senior Member, IEEE*, and Mount-Learn Wu

***Abstract*—This paper introduces a method combining a general electrothermal network π-model in system level and the associated mathematical technique, Green's theorem, in terms of the adopted materials and system geometries to build up an equivalent electrothermal circuit model (EETCM) for efficient thermal analysis and behavior prediction in a thermal system. Heat conduction and convection equations in integral forms are derived using the theorem and successfully applied for the thermal analysis of a 3-D optical stack, vertical-cavity surface-emitting lasers (VCSELs) on a silicon optical bench. The complex stack structure in conventional simulators can be greatly simplified using the method by well-predicting probable heat flow paths, and the simplification can eventually achieve the goal of CPU time saving without having complicated mesh designing or scaling. By comparing the data from the measurement, the finite-element simulation, and the method calculation shows that an excellent temperature match within $\pm\sim 0.5$ °C and 90% CPU time saving can be realized.**

***Index Terms*—3-D optical stacks, Green's theorem, conduction, convection, equivalent electrothermal circuit model (EETCM), general electrothermal network π-model, heat transfer equation, silicon optical bench (SiOB), thermal management, vertical-cavity surface-emitting laser (VCSEL).**

I. Introduction

HIGH SPEED, low power consumption, robust performance, and small form factor are four primary design issues in the development of the next generation microelectronic systems [1], [2]. However, undesired nonuniformly thermal effects due to drastic increase of the power dissipation within intensively operating chipsets have become significant design problems in the system development [1]–[4] and even restrained the design flexibility in terms of associated configurations of device packaging system and maximum power performance of integrated system circuits [1]. Several strategies and techniques concerned with the predictions of the undesired thermal effects on the microsystem performance and reliability have been presented to conquer the circumstance [1]–[8]. So far, the establishment of equivalent electrothermal circuit model (EETCM) is the most efficient thermal analysis scheme that can be easily implemented in computer-aided design (CAD) programs for optimal system-IC designs to avoid undesired system functionality degradation and device failure resulted by excess thermal accumulation. In comparison with the other analytical methods for the prediction of nonuniformly thermal effects, such as numerical solutions based on Laplace's equation [1], finite-element analysis (FEA), or boundary element method (BEM) for computer simulators [5]–[7], the EETCM can also effectively prevent data unwieldiness and time consuming in the thermal analysis resulted by the complicated boundary conditions (BCS) associated with a system configuration. The complexity of BCS will cause a large amount of meshing work in CAD simulation, which would affect the accuracy of outcomes and raise the analysis time and cost.

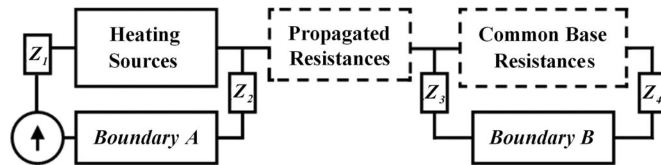

Fig. 1. Scheme of the general electrothermal network π-model for thermal management [8]. By analogy with the common electric circuit π-model, three main blocks, heating sources, propagated resistances, and common base resistances, are adopted to present the thermal sources, thermal flow paths, and the common base, respectively.

Therefore, for developing an efficient method for the thermal analysis of a microelectronic system with corresponding behavior predictions, this paper will illustrate a previously developed general electrothermal network π-model in the system level [8], as shown in Fig. 1. By employing the concept of the π-model in electronic transistors, a thermal system can be decomposed into three main subcomponents, which are heating sources, propagated resistances, and common base resistances, respectively. From the model, the thermal interconnects from one component to the others or to external boundaries can be definitely clarified, and the external boundaries connected to the main components can be decomposed into several thermal paths to simplify the BCS. Thence, by introducing Green's theorem for resolving the boundary problems in the Poisson's equation of power density and heat flux gradient, new heat conduction and convection equations in integral forms can be derived to clearly specify the thermal propagations within the system, and the thermal interactions between the system and its surrounding environment. Therefore, the thermal fields within the system and on the external surfaces under the prescribed thermal-field-BCS can be defined, as well as the temperature distribution of

Manuscript received July 8, 2010; revised August 31, 2010; accepted October 4, 2010. Date of publication December 16, 2010; date of current version June 8, 2011. This work was supported by the Optical Sciences Center, National Central University, Taiwan, under Project 99-EC-17-A-07-S1–001.

C. C. Chen, Y. C. Chen, and Y. T. Cheng are with the Microsystems Integration Laboratory, Department of Electronics Engineering and the Institute of Electronics, National Chiao Tung University, Hsinchu, Taiwan 300 (e-mail: gettgod.ee92g@nctu.edu.tw; ycchen.ee97g@g2.nctu.edu.tw; ytcheng@mail.nctu.edu.tw).

C.-T. Chen, H.-L. Hsiao, C.-C. Chang, and M.-L. Wu are with the Department of Optics and Photonics, Institute of Optical Sciences, National Central University, Jhong-Li, Taiwan 320 (e-mail: cs13579@hotmail.com; s972406006@dop.ncu.edu.tw; 972406010@cc.ncu.edu.tw; mlwu@dop.ncu.edu.tw).

Color versions of one or more of the figures in this paper are available online at http://ieeexplore.ieee.org.

Digital Object Identifier 10.1109/JSTQE.2010.2090037

1077-260X/$26.00 © 2010 IEEE

the system, which can help designers easily identify the hottest spot and the primary conducting paths of the heat flux in the system.

Since late 1980s, it has been proposed to utilize silicon substrate as a cost-effective optical bench to integrate optical and microelectronic components for gigabit per second (Gbps) high-speed optical data communication applications [9]–[11]. The implementation of the silicon optical bench (SiOB) can greatly shrink packaging size and electrical interconnection length accompanying the reduction of parasitic effects in the optical transceiver system for high-speed data communication applications. Meanwhile, the SiOB can provide several unique packaging characteristics including precise optical alignment for low coupling loss from optical components to fiber cores, small thermal mismatch between the components for high reliability of the chip system, excellent thermal conductivity of silicon substrate for good chip performance with better cooling, and exact passive fabrication for good impedance matching of signal transmission within components. Nevertheless, SiOB still has its intrinsic shortcomings. Silicon is a lossy substrate material in the RF/microwave/millimeter wave regime. Electrical signals transmitted between on-chip circuitries can be easily coupled into silicon substrate to generate substrate noise. Electrical loss resulted by induced eddy current in the substrate would degrade the performance of passive components in the circuitry. In order to resolve the issue, a thick layer of dielectric, such as silicon oxide, nitride, or benzo-cyclo-butene (BCB), is utilized as an electrical insulator for passive device fabrication, where the loss can be greatly reduced [8]. Owing to the high thermal-resist characteristic of the dielectrics, laser diode directly mounted on the top of them would have an inevitable working temperature raise that could affect the laser performance.

In this paper, an EETCM established according to the network π-model is presented for the thermal behavior analysis of the SiOB. A four-channel vertical-cavity surface-emitting laser (VCSEL, BeamExpress, SA.) array is flip-chip bonded using Au–Sn solder with the SiOB as a Gbps optical transmitter, where transmission lines are fabricated as electric interconnects, as shown in Fig. 2. The SiOB is monolithically fabricated with a 45° microreflector [see Fig. 2(b)] and a V-groove array that can incorporate optical fibers with itself [see Fig. 2(c)]. The reflectors and V-grooves can provide precise optical alignment and coupling between fibers and VCSELs, simultaneously. Detail SiOB design consideration and fabrication process can be referred to [11]. Using the presented network π-model and the EETCM, the thermal behavior in the system and the interaction between the system and the surrounding environment can be well predicted, and the simplification of the geometrical structure used in the simulators is likewise achieved to provide a quick solution for the optical system optimization as well as thermal management.

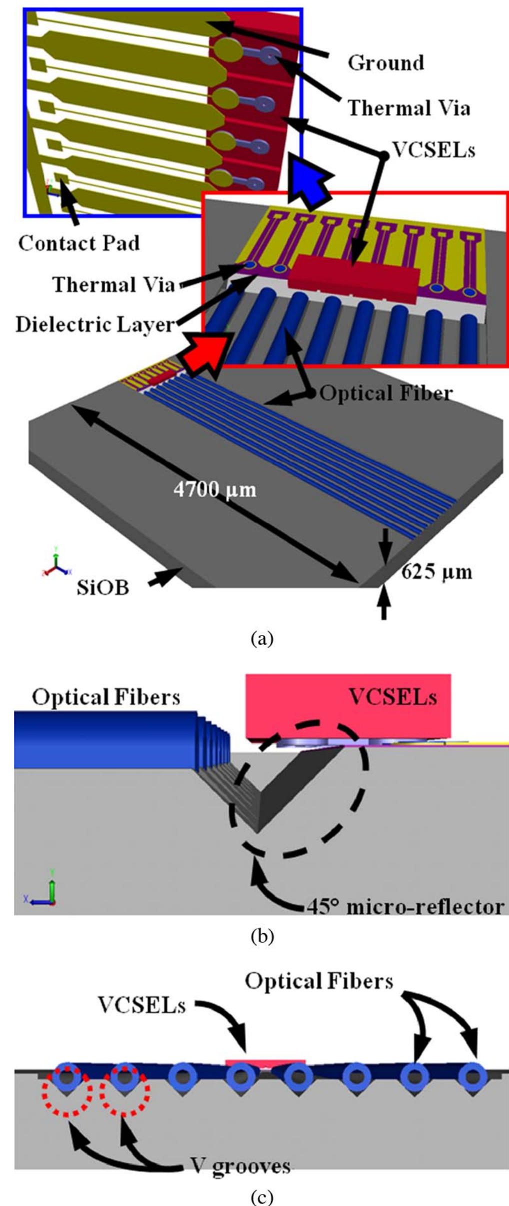

Fig. 2. (a) Scheme of the 3-D-stacked VCSELs on a SiOB. It is obviously that there should be complicated thermal behavior inside the SiOB due to its large volume and aspect ratio. The insertion of upper right corner shows complicated structure of the VCSELs, the adjacent contact pads, and the thermal via in detail. The insertion of upper left corner shows the bottom structure of the VCSELs and the interconnected thermal conducting channels. The detail profiles of the (b) 45° micro-reflector and the (c) V-groove array that are monolithically fabricated on the SiOB.

II. Thermal Analysis of VCSELs on an SiOB

Three main blocks labeled with heating sources, propagated resistances, and common base resistances in the general electrothermal network π-model, as shown in Fig. 1, represent the thermal sources, the thermal flow paths, and the common base of thermal conducting system, respectively. The dash lines enclosing each presented blocks in the network π-model represent an adiabatic surface [1]. The impedance parameters Z_i, where i represents 1, 2, 3, and 4, can be defined as the thermal resistance of heating source itself, nature or forced air convection, thermal capacitance, and other specified BCS, etc. *Boundaries A* and *B* can be the common base of the thermal flows, other heating components of thermal conducting system with specified thermal conditions, external boundaries, or interconnections

between different systems. It should be noted that icons of the source of thermal flow and the block of heating source represent the generation and direction of the thermal flow and the main heated component, respectively. As the three main blocks are definitely determined, the impedance parameters and boundaries can be specified and derived according to the configuration of the thermal system. The model can provide the flexibility in resolving the analysis complexity of the thermal impedance and the external boundary problems. Additionally, the BCS associated with their thermal behaviors could be further substituted by the presented thermal impedances or *Boundary A* (or *B*). Thus, the thermal behaviors could be likewise calculated qualitatively and quantitatively by means of the Fourier's law or the following Green's theorem in terms of temperature distribution.

Thermal phenomena of a long-wavelength VCSEL are complicated due to its complex multilayered configuration, containing an active region with several strained quantum wells followed by a sandwiched layer, in which a heavily doped p–n tunnel junction is embedded in two GaAs-based distributed Bragg reflectors (DBRs) in our case [12]. Thus, the thermal phenomena take place within the volume during operation will include the mutually interrelated optical, electrical, thermal, and electron-hole recombination phenomena [13]–[15]. Meanwhile, anisotropic thermal behaviors from the nonuniformly multilayered configuration are limited by the structural geometry of the VCSEL, therefore an effective thermal conductivity should be adopted for replacing the conventional values of each layers in the configuration [16], [17]. In addition, the nature and location of each heat source in the VCSEL are also critical characteristics, because the Joule heating is equally important as the active region and DBRs heating in the VCSEL [18], [19]. Therefore, the source of thermal flow and the Z_1 as shown in Fig. 1 are merged into the block of heating source for definitely specifying the exact location of the heating source. The location of the thermal flow source is assumed at the geometrical center of the VCSEL. Meanwhile, the complicated mutually interrelated thermal phenomena will be tentatively substituted with an electricthermal energy transfer efficiency coefficient for the steady state in the system level. In this paper, an effective thermal conductivity of the VCSEL with the value of 44 W/m·K is utilized for the EECTM model in the thermal analysis.

Fig. 3(a) and (b) show the electrothermal network π-model and the associated EETCM of the aforementioned 3-D-stacked VCSELs on the SiOB, respectively. The two parameters, the source of thermal flow and the Z_1, are the components of the heating source in the network π-model since the VCSELs are the main thermal generators and also the main heated components in the case. The parameters Z_1 and Z_2, Z_3, and Z_4 are thermal resistances of the 3-D-stacked VCSEL ($R_{\rm VCSEL}$ and $R'_{\rm VCSEL}$), an infinite thermal resistance due to the negligence of nature air convection, and the thermal capacitance of SiOB ($C_{\rm SiOB}$), respectively. Both the *Boundaries A* and *B* are the common bases of thermal flows for the entire thermal conducting system. Additionally, the blocks of propagated resistances are represented by a serial connection of gold ($R_{\rm Gold}$) and BCB ($R_{\rm BCB}$) layers, which is parallel connected with air ($R_{\rm Air}$). The common base resistance is the SiOB ($R_{\rm SiOB}$). Four switches adopted for the

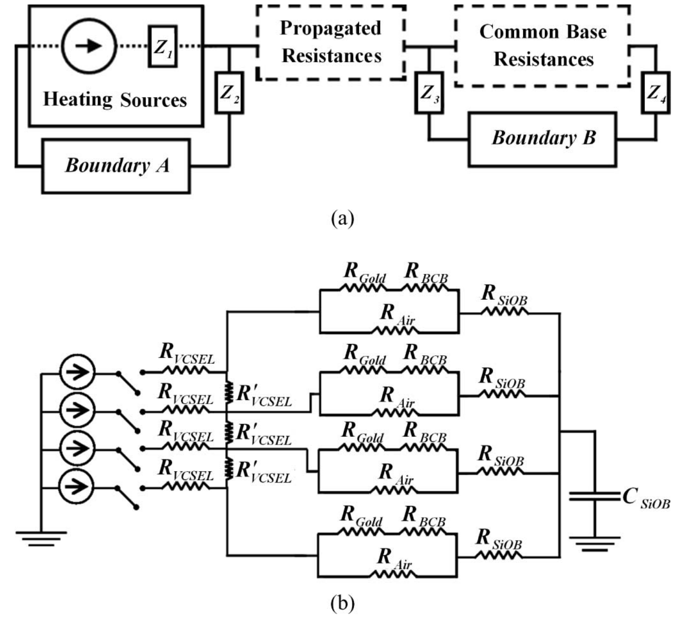

Fig. 3. (a) Scheme of the modified general electrothermal network π-model. The source of thermal flow and Z_1 are the components of the heating source due to the VCSELs are main heating generators themselves in our case. (b) EETCM of the VCSELs on the SiOB, where Z_1 and Z_2, Z_3, and Z_4 are thermal resistances of VCSEL ($R_{\rm VCSEL}$ and $R'_{\rm VCSEL}$), an infinite thermal resistance due to without nature air convection here, and the thermal capacitance of SiOB ($C_{\rm SiOB}$), respectively.

TABLE I
THE DIMENSION PARAMETERS AND THERMAL CONDUCTIVITIES OF THE ADOPTED MATERIALS

Layer	Material	Thickness (μm)	Area (μm^2)	Thermal Conductivity (W/m-K)
SiOB	Silicon	625	4.7×10^7	148
Dielectric layer	BCB	3	2000×1070	0.29
Thermal via	Gold	12	45×45×π	318
Contact pad	Gold	10	3.2×10^4	318
VCSEL	GaAs	150	250×350	44 [17]
Ground	Gold	10	1.6×10^6	318

sources of thermal flow indicate the VCSELs can be individually operated. In fact, it is the degree of freedom in arranging the thermal impedances in the model as aforementioned. According to the Fourier's conduction law, $R_{\rm VCSEL}$, $R'_{\rm VCSEL}$, $R_{\rm Gold}$, $R_{\rm Air}$, and $R_{\rm BCB}$ can be easily calculated as t_j/k_jS_j, where *j, t, k,* and *S* are the adopted material, thickness, thermal conductivity, and contact area of the materials, respectively. $C_{\rm SiOB}$ is equal to $Q/\Delta T$, where Q and ΔT represent dissipated power and temperature difference between the bottom of the SiOB and ambient environment, respectively. For the purpose of convenient and fair comparison, Table I shows the dimension and thermal conductivity of each adopted material utilized in both of the model calculation and the simulation.

Generally, after obtaining all thermal characteristics of the components in the thermal conducting system, paths of thermal flux and the highest temperature on the system can be uniquely and rapidly determined using the presented EETCM. The

thermal behaviors within the heating sources (the 3-D-stacked VCSELs), however, are always more complicated than the other components, since they are also the power generators in the system and simultaneously contact the surfaces of the internal system and the external environment. Thus, it is necessary to employ a new mathematical technique to exactly evaluate the temperature distribution on these contacted surfaces. By realizing the requirement, the mathematical technique of the Green's theorem is adopted in the paper to sufficiently and qualitatively describe the thermal characteristics of the 3-D-stacked optical transmitter.

III. Heat Transfer Equations in Integral Forms

A. Green's Theorem

Green's theorem is a mathematical tool for dealing with the problems of specified BCS fixing the field values at all points in the interesting volume [20]–[23]. As long as field sources within the volume and net field flux on the surfaces enclosing the volume are known, the physical characteristics of the field inside the volume can be uniquely determined as well as the transfer properties on the surrounding surfaces. Differing from the previously presented graphical method of the finite-difference equations [24], Green's theorem provides more degrees of freedom for dealing with the problems of isothermal surfaces. Once isothermal surfaces of a heating system are predicted, heat conduction flux as well as adiabatic surfaces could be likewise quantitatively determined. Thus, Green's theorem is one of the candidates to mathematically and physically define the thermal characteristics of the presented EETCM of the 3-D-stacked optical transmitter.

Starting from the second Green's theorem [22]

$$\int_v \left[\varphi(\bar r')\nabla'^2\psi(\bar r') - \psi(\bar r')\nabla'^2\varphi(\bar r')\right] d\,V' = \oint_s \left[\varphi(\bar r')\nabla'\psi(\bar r') - \psi(\bar r')\nabla'\varphi(\bar r')\right]\cdot \hat n da' \quad (1)$$

where $\varphi(\bar r')$ and $\psi(\bar r')$ are two arbitrary scalar fields. The parameters $\bar r'$, V', $\hat n$, and a' are the position of the field source, the interesting volume, the normal unit vector of the surrounding surface enclosing the volume, and the surrounding surface, respectively. In order to describe the temperature distribution of the thermal characteristics of the heating system by means of the Green's theorem, the two scalar fields should beartificially chosen

$$\varphi(\bar r') = \frac{1}{|\bar r - \bar r'|} \quad (2)$$

and

$$\psi(\bar r') = T(\bar r') \quad (3)$$

where T and $\vec r$ are the temperature distribution and the observed point, respectively. By substituting (2) and (3) into (1), and using the identity

$$\nabla'^2\varphi(\bar r') = \nabla'^2\frac{1}{|\bar r - \bar r'|} = -4\pi\delta(\bar r - \bar r') \quad (4)$$

the temperature distribution is then calculated as follows:

$$T(\bar r) = -\frac{1}{4\pi}\int_v \frac{\nabla'^2 T(\bar r')}{|\bar r - \bar r'|}dV' + \frac{1}{4\pi}\oint_s\left[\frac{\nabla'^2 T(\bar r')}{|\bar r - \bar r'|} - T(\bar r')\nabla'\left(\frac{1}{|\bar r - \bar r'|}\right)\right]\cdot\hat n da'. \quad (5)$$

For simplifying the prescribed BCS, the surrounding surface a' can be flexibly assumed as an isothermal surface. Thus, temperature distribution of the third term in (5) becomes a constant distribution, and the Green's theorem for the temperature distribution can be further modified as a temperature difference

$$T(\bar r) - T(\bar r') \equiv \Delta T = -\frac{1}{4\pi}\int_v \frac{\nabla'^2 T(\bar r')}{|\bar r - \bar r'|}dV + \frac{1}{4\pi}\oint_s \frac{\nabla' T(\bar r')}{|\bar r - \bar r'|}\cdot\hat n da'. \quad (6)$$

Eventually, the difference of temperature distribution for a heating system with prescribed BCS could be clarified in detail by treating the volume and surface integrals in (6) carefully.

B. Heat Conduction Equation

By analogy with the Poisson and electric-field equations in a steady state [22], the thermal sources in the volume and surface integral in (6) can be modified as follows:

$$\nabla'^2 T(\bar r') = -\frac{q_V}{k_V} \quad (7)$$

and

$$\nabla' T(\bar r') = -\frac{q_S}{k_S}\left(\hat r - \hat r'\right) \quad (8)$$

where q_V and q_S are the volume power density in W/m^3 generated within the interesting volume and the surface power density in W/m^2 radiated from the surrounding surface, respectively. The k_V and k_S are the thermal conductivity in W/m·K for volume and surface integrals, respectively. As the physical meanings of the conduction, the power densities mentioned in (7) and (8) represent the volume and surface densities of the thermal sources at specified points, respectively. Therefore, it indicates that the power densities of the conduction heat transfer also obey the Gauss's law.

By substituting (7) and (8) into (6), the difference of temperature distribution for the heat conduction, as shown in Fig. 4 can be derived as follows:

$$\Delta T = \frac{1}{4\pi}\int_V \frac{q_V}{k_V|\bar r - \bar r'|}dV' - \frac{1}{4\pi}\oint_S \frac{q_S\left(\hat r - \hat r'\right)\cdot\hat n}{k_S|\bar r - \bar r'|}da'. \quad (9)$$

For constant power density and isotropic thermal conductivity, (9) could be further simplified by setting the field source on the original point

$$\Delta T = \frac{q_V}{3k_V}|\bar r - \bar r'|^2 - \frac{q_S}{k_S}|\bar r - \bar r'|\left(\hat r - \hat r'\right)\cdot\hat n. \quad (10)$$

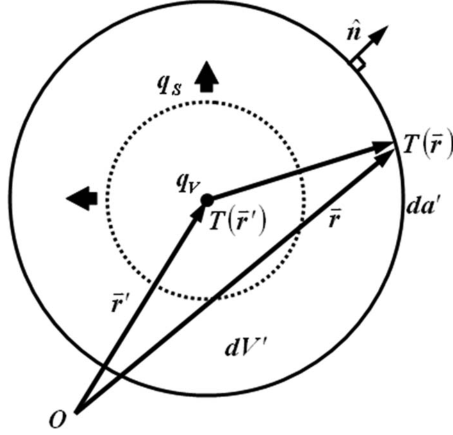

Fig. 4. Scheme of conduction heat transfer sphere with specified volume and surrounding surface. The parameters q_v and q_s are the volume power density in W/m^3 generated within the interesting volume and surface power density in W/m^2 radiated from the surrounding surface, respectively. The propagation direction of the surface power density is outward and parallel with the normal unit vector. The difference of the temperature distribution could be well determined using the derived conduction heat transfer equation in integral form.

Physically and conceptually, (10) could be simply tackled as a one-dimension problem by assuming $3k_V = k_S = k$ and realizing the vector difference to be the thermal conducting path ΔL, and it will become

$$\Delta T = \frac{q_V}{k}\Delta L^2 - \frac{q_S}{k}\Delta L\left(\bar{r} - \bar{r}'\right)\cdot\hat{n} \tag{11}$$

or

$$k\frac{\Delta T}{\Delta L} = q_V\Delta L - q_S\left(\hat{r} - \hat{r}'\right)\cdot\hat{n} \equiv q\Delta L - q_n. \tag{12}$$

Equation (11) indicates that the subtraction of the power density radiated from the surrounding surface from the power density generated within the interesting volume will be equal to the product of the temperature gradient and the thermal conductivity in one-dimension for the case in a steady state. In a source free volume, (12) definitely becomes the so-called Fourier's law in heat conduction [24] that also validates the correction of the equality assumption of $3k_V = k_S = k$. The aforementioned (9) is, thus, the integral form of the heat conduction equation. Meanwhile, the thermal resistances specified in the EETCM shown in Fig. 3(b) can be derived as follows:

$$R = \left[3q\int_V \frac{dV'}{|\bar{r} - \bar{r}'|} - q_n\oint_S \frac{da'}{|\bar{r} - \bar{r}'|}\right] \Big/ \left[4\pi k q_n \int_S \left(\hat{r} - \hat{r}'\right)\cdot\hat{n}da'\right]. \tag{13}$$

C. Heat Convection Equation

By recalling (6) and considering that there is no power source in the mechanism of heat convection, the temperature difference resulted by the convection, as shown in Fig. 5, can be described as follows:

$$\Delta T = \frac{1}{4\pi}\oint_S \frac{\nabla' T\left(\bar{r}'\right)}{|\bar{r} - \bar{r}'|}\cdot\hat{n}'da'. \tag{14}$$

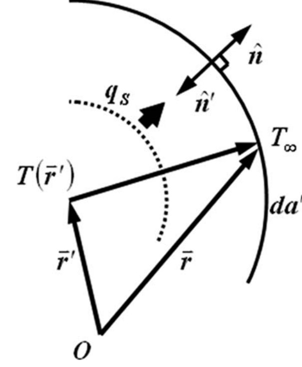

Fig. 5. Scheme of convection heat transfer sphere with specified surrounding surface. The propagation direction of the surface power density is outward and antiparallel with the normal unit vector $\hat{n}'$. The difference of the temperature distribution could be well determined using the derived convection heat transfer equation in integral form.

Slightly different from the definition of the surrounding surface in (9), the surface of heat convection mechanism could be extended to the surrounding, where the surface temperature T_∞ maintains as a constant and will not be influenced by the internal heating systems. Thus, by substituting (8) into (14), the temperature distribution resulted by the heat convection can be obtained by the derived temperature difference. Using similar approaches of (10) and (11), the temperature difference can be simplified as follows:

$$\Delta T = -\frac{q_S}{k}\Delta L\left(\bar{r} - \bar{r}'\right)\cdot\hat{n}' = \frac{q_n}{h} \tag{15}$$

or

$$q_n = h\Delta T = h\left[T\left(\bar{r}'\right) - T_\infty\right] \tag{16}$$

where h is $k/\Delta L$ and called the convection heat transfer coefficient in W/m$^2\cdot$K. It is noted that the direction of the normal unit vector $\hat{n}'$ is inward to the surface and opposite to the direction of the $\hat{n}$. Equation (16), therefore, becomes the so-called Newton's Law of cooling [24], and then, (14) is the integral form of the heat convection equation.

It is noted that there are three physical mechanisms of heat transfer for the heating system, i.e., conduction, convection, and radiation. Although the integral forms of the conduction and convection mechanisms have been qualitatively derived previously, the mechanism of the radiation is still not clearly defined in this paper. The difficulty to definitely determine the integral form of the radiation is due to its nature of the heat transfer. Being different from the mechanisms of the conduction and convection, i.e., random molecular and bulk motions of fluid, only an isothermal surface should be undertaken in the integral. The mechanism of the radiation has to deal with the energy interchanges between two surfaces from the system and the surrounding environment, respectively. Thus, it needs the Green's theorem with more complicated configuration. Fortunately, according to the Stefan–Boltzmann law, the radiation mechanism only can dominate at a very high temperature region, therefore, the mechanism can be neglected in the case concerned in the microelectronic systems [24]. At final, it is more convenient to use the integral forms for the thermal analysis rather than the

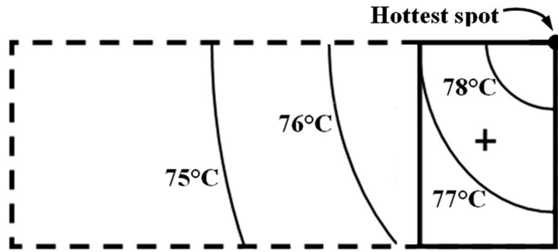

Fig. 6. Isothermal surfaces determined by means of the conduction and convection heat transfer equations. In the case, only the lateral single laser is turned on, where the heat source region is represented using the symbol "+". The input current is limited at 8 mA and the electricthermal energy transfer efficiency is 85.7% to meet the standard specification of the semiconductor-made VCSELs [25]. The theoretical temperature at the hottest spot is 78.4 °C.

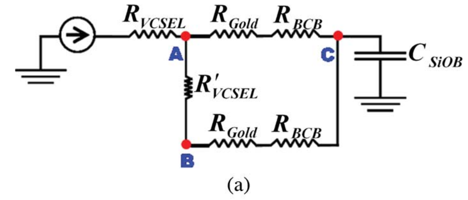

(a)

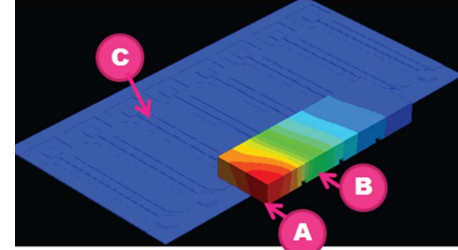

(b)

Fig. 7. (a) Scheme of the EETCM of simplified thermal conducting system with single operating VCSEL established by the network π-model. (b) Simulation result of simplified thermal conducting system. According the associated EETCM, the material of air and SiOB were removed in the system to reduce the required meshes as well as the CPU time and computer memory. The temperatures of node points A, B, and C are 78.9, 76.8, and 75 °C, respectively, while the input current is limited at 8 mA.

conventional Fourier's law and Newton's law of cooling, since these forms could easily elucidate the associated characteristics between the isothermal surface and the power density simultaneously in all thermal conducting components.

IV. Method Validation

A. Simulation Validation

Four VCSELs are stacked on a 625-μm-thick SiOB, which is operated in air without having artificial convection. The bottom of the SiOB is an isothermal surface, where it is set at 75 °C to imitate the operation environment of a typical optical transceiver system. All other surfaces are adiabatic, where no heat flux is allowed, as mentioned by the EETCM for the thermal analysis. According to the presented EETCM, as shown in Fig. 3(b), the contributions of thermal resistances of air within the propagated resistances and that of SiOB within the common base resistances could be ignored, since they have a large thermal resistance values in the part of parallel connection and a small resistance value in the part of serial connection, respectively. The materials of air and SiOB could be reasonably removed both in the model calculation and the CoventorWare simulation [7], therefore more than 80% reduction of required meshes can be achieved as well as the requirements of CPU time and memory operation in this case.

In the system, the hottest spot should be determined for realizing a reliable 3-D optical stack. Using the derived heat conduction and convection equations, the isothermal surface surrounding the source could be uniquely determined. The value of the volume power density in the source can be obtained by means of the product of the input power of the VCSEL per volume and its efficiency

$$q_V = \frac{I^2 R_h}{V_h}\eta \tag{17}$$

where I, R_h, V_h, and η are the input current, electric resistance of the heating source, volume of the heating source, and the electricthermal energy transfer efficiency coefficient, respectively. As shown in Fig. 6, while the lateral single laser is turned on, the configuration of the isothermal surfaces reveals the probable location of the hottest spot according to the calculation of the EETCM. After determining the hottest spot within or on the surface of the heating source, the temperature distribution could then be determined using (9) and (14) by evaluating the thermal distribution from the other two main components and the external BCS, which are surrounded by free air without artificial convection. The thermal resistance of each component can be also derived using (13). Fig. 7 shows the associated EETCMs and the simulation results after removing the air and SiOB in the thermal conducting system. Since the VCSELs have poor thermal conductivity than that of the thermal vias (see Table I), and the thickness of the operating VCSEL and the adjacent one can have two-order magnitudes larger than that of thermal vias, the thermal vias would become the main path of the thermal flow, as expected in this associated EETCM.

Meanwhile, the paths of the thermal flow depicted in Fig. 7 and extracted from the simplified thermal conducting system constructed in the simulation verify the validation of the EETCM by showing the possible paths of thermal flows on the main components. The simulation results cannot only obviously present the main paths of thermal flow as the prediction of the EETCM, but also indicate the hottest spot is at the outermost corner of the operating VCSEL. In the design and optimization stage, it is important to find out the hottest spot caused by a great quantity of thermal accumulation due to its direct correlation to undesired functionality degradation or even failure of the VCSELs in the optical system. In fact, according to the indications of the derived EETCM, the hottest spot could always take place at the joints of the heat source to the source of thermal flow, and the temperature in the spot strongly correlates to the characteristics of device material and geometry of Z_1 and the conditions of *Boundary A*, as shown in Fig. 7(a). Fig. 7(b) shows the simulation results, where the lateral VCSEL is operated with 8-mA input current and 2-V

bias voltage. The temperatures show at node points A, B, and C are 78.9, 76.8, and 75 °C, respectively. The hottest temperature at node A is close to the result that on the isothermal surfaces calculated by the EETCM, as shown in Fig. 6. The simulation results reveal that the hottest temperature happens at node A and the main path of thermal flow is from node A to C, which has an excellent match with the prediction of the simplified EETCM, as shown in Fig. 7(a). Therefore, for system-IC designers and engineers, the EETCM derived based on the electrothermal network π-model can indeed provide a quick and accurate way to analyze the worst cases at those joints by further investigating the thermal behaviors of Z_1 and *Boundary A*.

B. Apparatus Setup, Calibration, and Experimental Validation

InfraScope II, Thermal Imaging Microscope, (Quantum Focus Instruments Corp, Vista, CA) is employed for both thermal mapping and hot-spot detection in the measurement. Two main effects, vibration coupling and thermal air current, that could affect the measured accuracy have been carefully considered and controlled. The InfraScope is mounted on a vibration-isolated table and the measurement environment is located away from air flux. The entire 3-D VCSELs optical stack is fixed on the thermal stage of the InfraScope, where a bias temperature is set at 75 °C to imitate the conventional operation environment of typical optical transceiver systems. The optical stack starts with an unpowered state for measurement calibration. Radiance calibration is adopted to create the correlation between the output of infrared detector and the infrared radiance. The reference established in the unpowered state is used to calibrate the radiance units by accurately measuring the infrared radiation emitted by each pixel area of the optical stack. Then, the extracted emissivity map is utilized as a reference frame for each of the subsequent thermal images from the powered 3-D optical stack. The map can, therefore, be processed immediately for the temperature acquisitions. At final, by means of zooming in the region of the heating source adequately, i.e., the region of the VCSELs, the temperature distribution of the hot spot can be definitely determined, as well as the hottest temperature on the surface of the VCSELs.

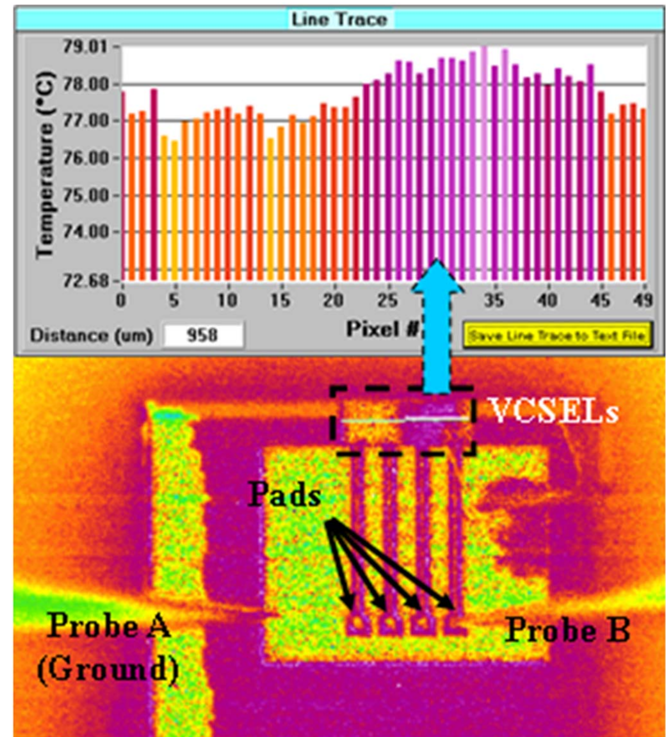

Fig. 8. Measured temperature distribution of SiOB heated by the operating VCSEL using IR microscope. Only a laser diode is operated by probe B with 8-mA input current and 2-V bias voltage.

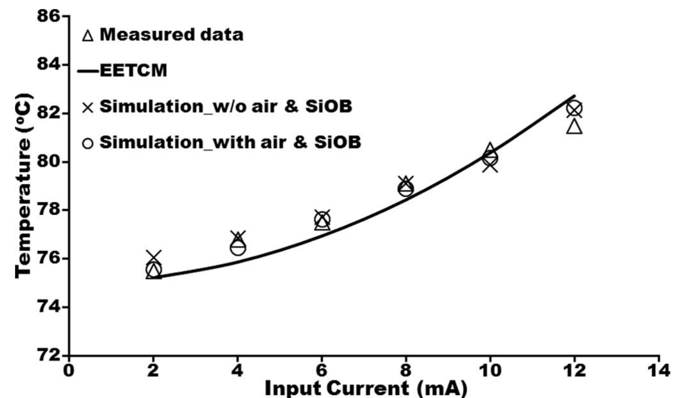

Fig. 9. Comparison between the EETCM with single laser turned on, measurement data, and simulated results with and without air and SiOB, respectively.

Fig. 8 is the detected infrared-ray (IR) thermal image that shows the temperature distribution of the SiOB heated by the singly operated VCSEL. The bottom of SiOB is constrained with a bias temperature of 75 °C for fair comparison. Only a laser diode is operated by probe B with 8-mA input current and 2-V biased voltage. The measured hottest temperature shown in Fig. 9 validate the simulation and model predictions, as shown in Figs. 6 and 7, respectively. The comparison between the CoventorWare simulation results with and without air and SiOB, respectively, also verify the simplification indicated by the EETCM. In order to further show the model accuracy in dealing with the thermal crosstalk between two operated lasers, Fig. 10 shows the thermal image of the optical transmitter, where two lasers are simultaneously operated. Each laser diode is operated with 8-mA input current and 2-V biased voltage. Fig. 11 shows the comparison between the measured data, the simulation, and the EETCM calculation. Excellent temperature matches within $\sim$0.5 °C verify the EETCM accuracy and show the practicality of the simplified structure, in which we can have 90% CPU operation time saving due to 80% mesh number reduction. In addition, the slight temperature mismatch should be caused by the thermal impedance mismatch between the interfaces and the phonon vibration. Further investigation and model improvement are still undergoing.

V. Conclusion

The paper physically and conceptually presents a method of thermal analysis by means of a general electrothermal network π-model in system level and an associated EETCM solved using

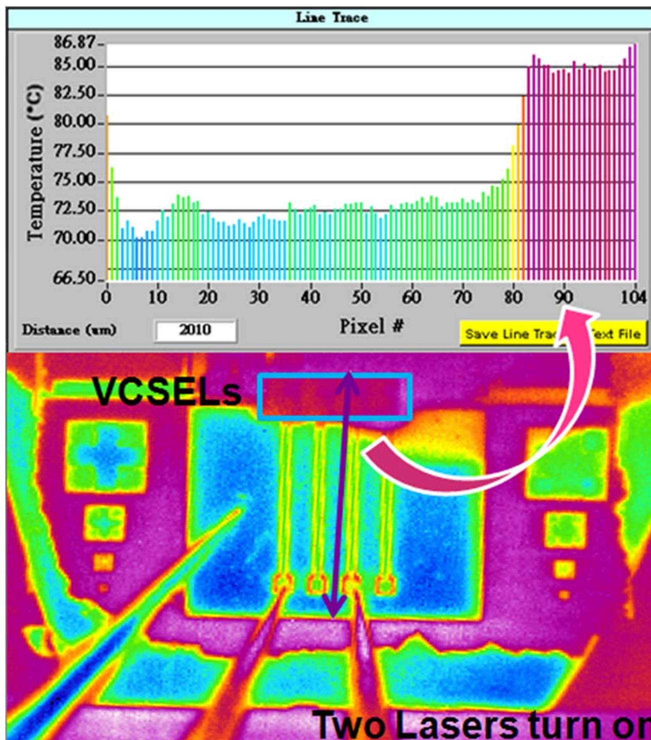

Fig. 10. Measured temperature distribution of SiOB heated by the operating VCSELs using IR microscope. Two laser diodes are operated with 8-mA input current and 2-V bias voltage.

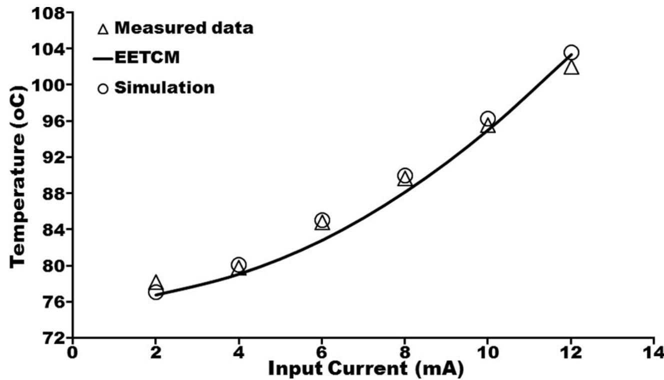

Fig. 11. Comparison between the EETCM with two lasers turned on, measurement data, and simulated result, respectively.

a proposed mathematical technique, the Green's theorem. By decomposing the thermal conducting system into three main components, a complex heating structure can be efficiently simplified without degrading the analytical accuracy. The derived heat conduction and convection equations in integral forms could help the designers and engineers realize the thermal behaviors within the integrated circuits and the thermal interconnections between the system and the external surrounding surfaces. By finding the isothermal surfaces within the heating source components, the hottest spot, and the probable paths of the thermal flow can be uniquely determined, therefore, the thermal system could be further optimized to avoid the device failure or breakdown. Furthermore, the associated circuit model can be readily used for design optimization via CAD programming in terms of the structure geometry and physical characteristics of materials used in the device or system. The model can also lead a way for structure simplification and system optimization with high accuracy and achieve the goal of CPU time saving in 3-D FEA simulation without complicated mesh studying or scaling.

Acknowledgment

All authors are grateful to the National Center for High-Performance Computing, Taiwan, for supporting computer software and facilities.

References

[1] A. M. Darwish, A. J. Bayba, and H. A. Hung, "Accurate determination of thermal resistance of FETs," *IEEE Trans. Microw. Theory Tech.*, vol. 53, no. 1, pp. 306–313, Jan. 2005.

[2] A. H. Ajami, K. Banerjee, and M. Pedram, "Modeling and analysis of nonuniform substrate temperature effects on global ULSI interconnects," *IEEE Trans. Comput.-Aided Des. Integr. Circuits Syst.*, vol. 24, no. 6, pp. 849–861, Jun. 2005.

[3] F. Tamigi, N. Nenadović, V. d'Alessandro, L. K. Nanver, N. Rinaldi, and J. W. Slotboom, "Modeling of thermal resistance dependence on design parameters in silicon-on-glass bipolar transistors," in *Proc. IEEE 24th Int. Conf. Microelectron.*, May, 2004, vol. 1, Serbia-Montenegro, pp. 257–260.

[4] B. Goplen and S. Sapatnekar, "Thermal via placement in 3D ICs," in *Proc. 2005 Int. Symp. Physical Des.*, Apr., pp. 167–174.

[5] K. Vanmeensel, A. Laptev, J. Hennicke, J. Vleugels, and O. Van der Biest, "Modeling of the temperature distribution during field assisted sintering," *Acta Materialia*, vol. 53, pp. 4379–4388, Aug. 2005.

[6] A. J. Kemp, G. J. Valentine, J.-M. Hopkins, J. E. Hastie, S. A. Smith, S. Calvez, M. D. Dawson, and D. Burns, "Thermal management in vertical-external-cavity-surface-emitting lasers: Finite-element analysis of a heat-spreader approach," *IEEE J. Quantum Electron.*, vol. 41, no. 2, pp. 148–155, Feb. 2005.

[7] CoventorWare (2008) [Online]. Available: http://www.coventor.com/, version 2008.

[8] C. C. Chen, C. Singh, Y. C. Chen, H.-L. Hsiao, C.-Y. Lee, M.-L. Wu, and Y. T. Cheng, "Equivalent electrothermal circuit model for vertical-cavity surface-emitting lasers on silicon optical bench," in *Proc. 15th Int. Workshop Therm. Investigat. ICs Syst. (THERMINIC)*, Leuven, Belgium, 7–9 Oct. 2009, pp. 8–12.

[9] I. P. Kaminow and T. L. Koch, *Opt. Fiber Telecommun. IIIB*. vol. 2, ch. 8, Boston, MA: Academic, 1997.

[10] C. Schuster, D. M. Kuchta, E. G. Colgan, G. M. Cohen, and J. M.Trewhella, "Package design and measurement of 10 Gbps laser diode on high-speed silicon optical bench," in *Proc. IEEE 12th Top. Meeting Electr. Perform. Electron. Packag.*, Princeton, NJ, 27–29 Oct.2003, pp. 63–66.

[11] H.-L. Hsiao, H.-C. Lan, C.-C. Chang, C.-Y. Lee, S.-P. Chen, C.-H. Hsu, S.-F.Chang, Y.-S. Lin, F.-M. Kuo, J.-W. Shi, and M.-L. Wu, "Compact and passive-alignment 4-channel × 2.5-Gbps optical interconnect modules based on silicon optical benches with 45° micro-reflectors," *Opt. Exp.*, vol. 17, pp. 24250–24260, Dec. 2009.

[12] VCSEL Technology, BeamExpress, SA. (2005). Wafer-fused VCSELs shape up for enterprise applications. Compound Semiconductor, [Online]. pp. 25–27. Available: http://www.beamexpress.com/publications.php.

[13] W. Nakwaski, "Principles of VCSEL designing," *Opto-Electron. Rev.*, vol. 16, pp. 18–26, 2008.

[14] W. Nakwaski and M. Osiński, "III: Thermal properties of vertical-cavity surface-emitting lasers," *Progr. Opt.*, vol. 38, pp. 165–262, 1998.

[15] L. Piskorski, R. P. Sarzala, M. Wasiak, and W. Nakwaski, "Tunning effects in optimization of GaAs-based InGaAs/GaAs quantum-dot VCSELs," *Opt. Commun.*, vol. 281, pp. 3163–3170, 2008.

[16] M. Wasiak and W. Nakwaski, "Effective thermal conductivity analysis of 1.55-μm InGaAsP/InP vertical-cavity top-surface-emitting microlasers," *Electron. Lett.*, vol. 29, no. 11, pp. 1015–1016, May 1993.

[17] W. Nakwaski, "Thermal conductivity of binary, ternary, and quaternary III-V compounds," *J. Appl. Phys.*, vol. 64, pp. 159–166, 1988.

[18] J. Piprek, T. Tröger, B. Schröter, J. Kolodzey, and C. S. Ih, “Thermal conductivity reduction in GaAs–AlAs distributed Bragg reflectors,” *IEEE Photon. Technol. Lett.*, vol. 10, no. 11, pp. 81–83, Jan. 1998.
[19] W. Nakwaski and M. Osiński, “Heat source distribution in etched-well surface-emitting semiconductor lasers,” *IEEE Photon. Technol. Lett.*, vol. 3, no. 11, pp. 979–981, Nov. 1991.
[20] R. Bialecki and A. J. Nowak, “Boundary value problems in heat conduction with nonlinear material and nonlinear boundary conditions,” *Appl. Math. Modelling*, vol. 5, pp. 417–421, Dec. 1981.
[21] M.-N. Sabry, “Static and dynamic thermal modeling of ICs,” *Microelectron. J.*, vol. 30, pp. 1085–1091, Nov. 1999.
[22] W. Greiner, *Classical Electrodynamics*. New York: Springer-Verlag, 1991.
[23] G. D. Mahan, *Many-Particle Physics*. New York: Plenum Press, 1981.
[24] F. P. Incropera and D. P. Dewitt, *Introduction to Heat Transfer*. New York: Wiley, 1996.
[25] 5 Gb/s 1310 nm waveband VCSEL, PRELIMINARY Datasheet, Beam Express, SA, [Online]. Available: http://www.beamexpress.com.

C. C. Chen was born in Taiwan. He received the B.S. degree in physics from the National Central University, Jhongli, Taiwan, in 2003, and the M.S. degree in electrical engineering from the National Chiao Tung University, Hsinchu, Taiwan, in 2006. His thesis was entitled, “A closed-form integral model of spiral inductor using the Kramers-Kronig relations.” He is currently working toward the Ph.D. degree at the Department of Electronics Engineering and the Institute of Electronics, National Chiao Tung University, where he is engaged in creating behavior models for solid-state Nano/ microelectromechanical systems devices and electromagnetic-thermal-field theory.

Y. C. Chen was born in Taiwan. He received the B.S. degree in electrical engineering from the National Taiwan Ocean University, Keelung, Taiwan, in 2006, and the M.S. degree in electronics engineering from the National Chiao Tung University, Hsinchu, Taiwan, in 2008. He is currently working toward the Ph.D. degree at the Department of Electronics Engineering and the Institute of Electronics, National Chiao Tung University, where he is engaged in microelectromechanical systems acoustic device.

Chin-Ta Chen received the B.S. degree in electronic engineering and M.S. degree in optical sciences from the National Central University, Taiwan, in 2008 and 2010, respectively, where he is currently working toward the Ph.D. degree at the Department of Optics and Photonics, Institute of Optical Sciences.

His research interests including optical interconnect and silicon photonics.

Hsu-Liang Hsiao received the B.S. degree in mechanical engineering and M.S. degree in optical sciences from the National Central University, Taiwan, in 2006 and 2008, respectively, where he is currently working toward the Ph.D. degree at the Department of Optics and Photonics, Institute of Optical Sciences.

His research interests including nano/micro optics, optical interconnect, and silicon photonics.

Chia-Chi Chang received the B.S. degree in physics from the National ChiaYi University, Taiwan, and the M.S. degree in optical sciences from the National Central University, Taiwan, in 2006 and 2008, respectively. He is currently working toward the Ph.D. degree at the Department of Optics and Photonics, Institute of Optical Sciences, National Central University, Taiwan.

His research interests include nano/micro optics, guided waves, and photonic integrated circuits.

Y. T. Cheng (SM’07) was born in Taiwan. He received the B.S. and M.S. degrees in materials science and engineering from National Tsing Hua University, Hsinchu, Taiwan, in 1991 and 1993, respectively, the M.S. degree in materials science and engineering from Carnegie Mellon University, Pittsburgh, PA, in 1996, and the Ph.D. degree in electrical engineering from the University of Michigan, Ann Arbor, in 2000. His Ph.D. thesis focused on the development of novel vacuum packaging technique for microelectromechanical systems (MEMS) applications.

He was in Army service in Taiwan for two years.He was a research staff member with IBM Thomas J. Watson Research Center, Yorktown Heights, where he was involved in several system-on-a-package (SoP) projects. In 2002, was an Assistant Professor at the Department of Electronics Engineering, National Chiao Tung University, Hsinchu, Taiwan, he is currently a Professor since 2009. His research interests include the fundamental study of materials for microsystem integration and nano/MEMS applications, SoP, and the design and fabrication of microsensors and microactuators.

Dr. Cheng was the corecipient of the 2006 Best Paper Award presented at the 13th IEEE International Conference on Electronics, Circuits and Systems. He is a member of Institute of Physics and Phi Tau Phi.

Mount-Learn Wu was born in Kaohsiung, Taiwan. He received the Ph.D. degree in optical sciences from National Central University, Jhong-Li, Taiwan, in 2001.

From 1999 to 2001, he was a Senior Engineer with the Universal Scientific Industrial Co., Ltd., Nan-Tou, Taiwan, where he was engaged in developing optical communication modules. From 2001 to 2005, he was with the Opto Tech Corp. and NeoStones MicroFabrication Corp., Hsinchu, Taiwan, where he was involved with the development of optical microelectromechanical systems for applications of optical communication, optical storage, electrophotography, and LED lighting. In August 2005, was an Assistant Professor at the Institute of Optical Sciences, National Central University, where currently an Associate Professor in the Department of Optics and Photonics since August 2009. His research interests include nano/microoptical system and silicon photonics.